Chemical Science

ROYAL SOCIETY OF CHEMISTRY

EDGE ARTICLE

View Article Online
View Journal | View Issue

Open Access Article. Published on 23 April 2025. Downloaded on 6/3/2026 1:37:08 PM.
This article is licensed under a Creative Commons Attribution-NonCommercial 3.0 Unported Licence.

Check for updates

Cite this: *Chem. Sci.*, 2025, **16**, 9195

All publication charges for this article have been paid for by the Royal Society of Chemistry

Stable cationic nanobelts synthesized by chemical oxidation of methylene-bridged [6] cycloparaphenylene†

Nobushige Kai,‡[a] Hideya Kono,‡[a] Timo Stünkel,[a] Daiki Imoto,[a] Riccardo Zanasi,*[b] Guglielmo Monaco,[b] Francesco F. Summa,[b] Lawrence T. Scott,[c] Akiko Yagi*[ad] and Kenichiro Itami*[de]

Received 19th February 2025
Accepted 4th April 2025

DOI: 10.1039/d5sc01305d

rsc.li/chemical-science

Nanobelts are cyclic arenes that only consist of annulated structures. Recently, various types of nanobelts have been synthesized and their unique properties have been unveiled. However, cationic nanobelts without heteroatoms have been rarely synthesized, and their properties are of significant interest from both fundamental and application perspectives. Herein, we report the synthesis of radical cationic and dicationic hydrocarbon nanobelts by chemical oxidation of methylene-bridged [6]cycloparaphenylene ([6]MCPP). These cationic species are remarkably stable in air, which made it possible to measure and uncover their structural and electronic properties. Notably, the [6]MCPP dicationic salt has sharp absorption and fluorescence bands at longer wavelengths than those of neutral [6]MCPP, close to the near-infrared region. From both experimental and theoretical investigation, the existence of a strong diatropic belt current in [6]MCPP dication was indicated. In addition, a longer lifetime was observed for the hexamethyl[6]MCPP dicationic salt than for the [6]MCPP dicationic salt in solution.

Cationic molecules have long been studied as reaction intermediates in a range of cation-triggered organic transformations and also have been utilized in numerous materials such as dyes, liquid crystals, conducting polymers, and photocatalysts.[1] Among them, cationic arenes, in which π-electrons have been removed from aromatic rings, have been recognized as important cationic molecules because they can act as intermediates of charge carriers in p-type organic semiconductors.[2] To utilize intrinsically moisture-sensitive cationic arenes as stable species, electron-donating heteroatoms such as nitrogen and oxygen atoms are often introduced into arene scaffolds. In contrast, cationic arenes without heteroatoms, namely cationic aromatic hydrocarbons, are relatively rare.[3] While the introduction of multiple bulky substituents such as mesityl groups to gain air-stability has been a common strategy in the field, this sometimes is not enough to stabilize cations of π-conjugated arenes. Delocalization of positive charge is another powerful strategy for stabilizing cationic species of π-extended arenes. In the past decade, the groups of Jasti and Yamago have extensively studied the cationic species of cycloparaphenylenes (CPPs) and other charged CPP derivatives, revealing their unique size-dependent properties.[4] Considering the recent progress of the chemistry of π-extended arenes,[5] their cationic species are also worth investigating.

Nanobelts and aromatic belts are a class of synthetically challenging and recently emerging cyclic π-extended arenes (Fig. 1a).[6,7] Since the first synthesis of (6,6)carbon nanobelts ((6,6)CNB) in 2017,[6] different types of nanobelts have been synthesized, and their properties have been investigated. Despite the recent advances in nanobelts, cationic nanobelts are limited to certain dicationic/tetracationic species of non-alternant nanobelts doped with nitrogen atoms and bowl-shaped nanobelts.[8] There are no reports on the synthesis of stable cationic species of nanobelts, probably because of their assumed instability; thus, their synthesis is in strong demand.

Herein, we report the synthesis of stable cationic hydrocarbon nanobelts. Methylene-bridged [6]cycloparaphenylene ([6]MCPP) was selected as our target nanobelt for obtaining a cationic nanobelt.[9] [6]MCPP is a nanobelt synthesized by our group in 2020, in which all the benzene rings of [6]CPP are bridged by methylene units. The synthesis of [6]MCPP requires only two steps from pillar[6]arene,[10] which has enabled the

[a]Department of Chemistry, Graduate School of Science, Nagoya University, Chikusa, Nagoya 464-8602, Japan. E-mail: yagi.akiko@itbm.nagoya-u.ac.jp
[b]Dipartimento di Chimica e Biologia "A. Zambelli", Università, Degli Studi di Salerno, Fisciano 84084, SA, Italy. E-mail: rzanasi@unisa.it
[c]Department of Chemistry, University of Nevada, Reno, Nevada 89557-0216, USA
[d]Institute of Transformative Bio-Molecules (WPI-ITbM), Nagoya University, Nagoya 464-8602, Japan
[e]Molecule Creation Laboratory, RIKEN Cluster for Pioneering Research, Wako, Saitama 351-0198, Japan. E-mail: kenichiro.itami@riken.ac.jp

† Electronic supplementary information (ESI) available. CCDC 2359239. For ESI and crystallographic data in CIF or other electronic format see DOI: https://doi.org/10.1039/d5sc01305d

‡ These authors contributed equally.

Open Access Article. Published on 23 April 2025. Downloaded on 6/3/2026 1:37:08 PM.
This article is licensed under a Creative Commons Attribution-NonCommercial 3.0 Unported Licence.

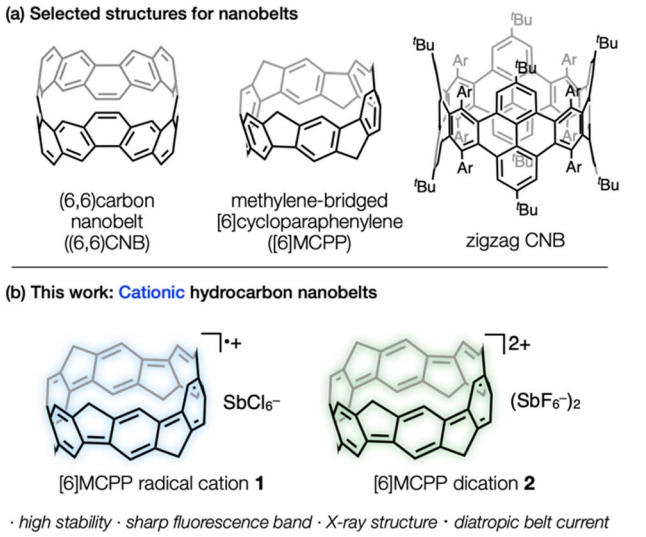

Fig. 1 (a) The structures of neutral aromatic hydrocarbon nanobelts. Ar = p-^{t}BuC$_6$H$_4$. (b) The structures of [6]MCPP radical cation $SbCl_6^-$ salt **1** and [6]MCPP dication $(SbF_6^-)_2$ salt **2**.

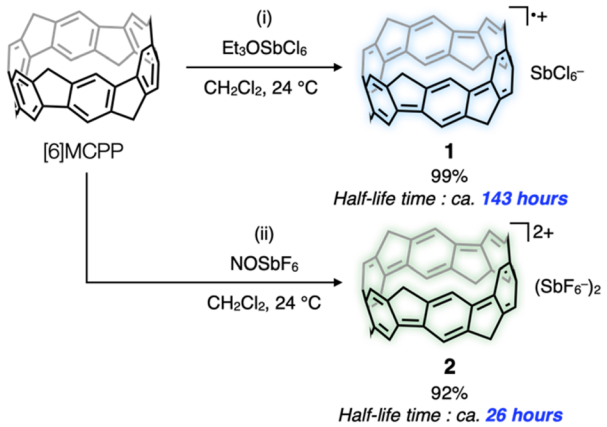

Scheme 1 Synthesis of **1** and **2**. Reaction conditions: (i) [6]MCPP (9.6 μmol, 5.1 mg, 1.0 equiv.), Et_3OSbCl_6 (14 μmol, 6.2 mg, 1.5 equiv.), CH_2Cl_2 (2.0 mL), 30 min. (ii) [6]MCPP (7.6 μmol, 4.0 mg, 1.0 equiv.), $NOSbF_6$ (23 μmol, 6.0 mg, 2.2 equiv.), CH_2Cl_2 (3.0 mL), 2 hours. Half-life time was determined in CH_2Cl_2 solution at 23 °C under air.

large-scale synthesis and commercialization of [6]MCPP.[11] Unique properties of [6]MCPP, such as a small energy gap (2.66 eV) and paratropic belt current, have led the progress of MCPP chemistry, as demonstrated by the syntheses of larger MCPPs ([8]MCPP and [10]MCPP),[12] a naphthalene-based MCPP,[13] and functionalized MCPPs.[14] Owing to the high highest occupied molecular orbital (HOMO) energy (−4.40 eV), electron-donating methylene units, and rigid cyclic π-conjugated system of [6]MCPP, we anticipated that cationic species of [6]MCPP can be easily and stably produced under air. The [6]MCPP radical cation $SbCl_6^-$ salt **1** and [6]MCPP dication $(SbF_6^-)_2$ salt **2** were synthesized and found to be very stable as solutions in CH_2Cl_2 and even as solids in air. Nuclear magnetic resonance (NMR) analysis, ultraviolet (UV)–visible (vis)–near-infrared region (NIR) absorption/fluorescence measurements, X-ray crystal structure analysis, and electron spin resonance (ESR) measurement of **1** and **2** revealed several unique properties of the cationic nanobelts.

Chemical oxidation of [6]MCPP with 3 equivalents of $NOSbF_6$ in CH_2Cl_2 solution, at 23 °C under an argon atmosphere, changed the red color of the reaction solution, derived from [6]MCPP, to a yellow green color. From ^{1}H NMR, ^{13}C NMR, and electrospray ionization (ESI) mass spectrometric analyses, as well as UV–vis–NIR absorption measurements, the full conversion of [6]MCPP was observed and **2** was obtained in 92% isolated yield (Scheme 1, bottom). When using **1** equivalent of $NOSbF_6$, the formation of **1** was indicated by the ESR and absorption spectra of the reaction mixture. Eventually, under these conditions, **1** was isolated in 73% yield (see the Section 2.1 in ESI† for details). By treating [6]MCPP with Et_3OSbCl_6, a slightly weaker oxidant than $NOSbF_6$ (E_{ox}; 0.87 V and 0.91 V (*vs.* Fc/Fc$^+$), respectively), **1** was also selectively formed as judged by ESR analysis and absorption measurements and isolated in 99% yield (Scheme 1, top). In the ESR spectrum of the CH_2Cl_2 solution of **1** measured under argon, the g value of **1** is 2.0037 (329.059 mT) and the hyperfine structure was observed, which are reasonable based on the results reported for [n]CPP radical cations (see Fig. S14 in ESI†). The half-life time of **1** and **2** are determined as about 143 hours and 26 hours, respectively, from the decay of the maximum absorption peak intensities in CH_2Cl_2 solution under air (see Fig. S1 and S2 in ESI†). The determined values of half-life time should be longer than those of CPP cations, which have been characterized as air-sensitive; however, no lifetime data have been reported.[4] The comproportionation reaction by mixing **2** and neutral [6]MCPP was conducted in CH_2Cl_2 at room temperature. This oxidant-free method of generating the radical cation was previously reported in the case of CPP by the Yamago group.[4d] As a result, **1** was obtained quantitatively, also supporting high stability of **1** (see the Section 2.4 in ESI†).

A single crystal of **2** was successfully obtained by slow evaporation of a CH_2Cl_2 solution at −30 °C under an argon atmosphere for 6 days. X-ray single-crystal structural analysis revealed the crystal structure of **2** (Fig. 2a) and its packing structure, where the [6]MCPP^{2+} scaffold is aligned in columns with two sandwiched SbF_6^- anions and CH_2Cl_2 molecules

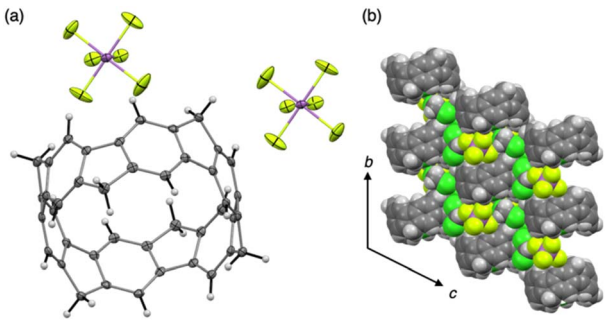

Fig. 2 X-ray crystal structure of **2**. (a) Oak Ridge Thermal Ellipsoid Plot (ORTEP) drawing of **2** with 50% thermal probability. (b) Packing structure viewed along the a-axis.

 © 2025 The Author(s). Published by the Royal Society of Chemistry

Open Access Article. Published on 23 April 2025. Downloaded on 6/3/2026 1:37:08 PM.
This article is licensed under a Creative Commons Attribution-NonCommercial 3.0 Unported Licence.

Table 1 Structure index of **2** and comparison with [6]MCPP

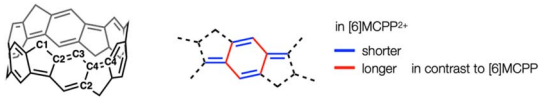

	[6]MCPP	[6]MCPP^{2+}	Δ([6]MCPP^{2+}–[6]MCPP)
Diameter [Å]	7.758	7.675	−0.083
C1–C2 [Å]	1.518	1.514	−0.004
C2–C3 [Å]	1.384	1.368	−0.016
C2–C4 [Å]	1.408	1.436	0.028
C3–C4 [Å]	1.395	1.415	0.020
C4–C4 [Å]	1.478	1.428	−0.050

(Fig. 2b).[15] The diameter of the [6]MCPP^{2+} scaffold is estimated as 7.675 Å, which is 0.083 Å shorter than that of neutral [6]MCPP (Table 1). Considering the carbon–carbon bonds, the difference between **2** and [6]MCPP strongly indicates that the [6]MCPP^{2+} scaffold has a quinoidal character. The harmonic oscillator model of aromaticity (HOMA) values for the 6-membered rings are estimated using the crystal structures of [6]MCPP and **2**, and density functional theory (DFT) calculations at the B3LYP/6-31G(d) level of theory (see the Section 5 in ESI† for details). The average HOMA value is 0.702 for [6]MCPP^{2+} scaffold in contrast to 0.955 for [6]MCPP, supporting the decreased benzenoid character of **2**. This difference was also observed in the case of cationic CPPs, which explains the effective delocalization of the positive charge across the entire [6]MCPP^{2+} scaffold.

The UV–vis–NIR absorption and fluorescence spectra of **1** and **2**, in CH_2Cl_2 solutions, are recorded and compared with those of [6]MCPP (Fig. 3a). For **1**, four absorption peaks are observed at 415, 890, 1037, and 1054 nm. The absorption band in the NIR region clearly indicates the radical cationic character of **1**, which undergoes transitions with a singly occupied molecular orbital (SOMO). Using DFT calculations, the frontier molecular orbitals of **1** and **2** were depicted and the features similar to those seen in most of radical cations and cations were found. The SOMO of **1** is distributed exactly the same way as the HOMO of [6]MCPP, and the other frontier molecular orbitals of **1** are shifted by one (see Fig. 3b and S10 in ESI†). Similarly, the LUMO of **2** has the same orbital distribution as that of the HOMO of [6]MCPP, whereas the other orbitals are shifted by one. As estimated by time-dependent DFT (TDDFT) calculation at the UB3LYP/6-31G(d) level of theory, the absorption bands of **1**, with peaks at approximately 415 nm, 890 nm, 1037 nm and 1054 nm can be attributed to HOMO/HOMO−1 to LUMO, and SOMO → LUMO, HOMO/HOMO−1 → SOMO transitions, respectively, though the absorption at 890 nm is very weak, presumably because SOMO → LUMO transition is forbidden ($f = 0$). Fluorescence of the CH_2Cl_2 solution of **1** was measured but not observed.

The absorption bands of the CH_2Cl_2 solution of **2** are observed with peaks at 453 and 745 nm. The positions of the peaks correspond well with the HOMO/HOMO−1 → LUMO+1 (415 nm) and HOMO/HOMO−1 → LUMO (701 nm) transitions calculated using TDDFT. Notably, the absorption band with a peak around 745 nm is very sharp with a full width at half maximum (FWHM) of 14.5 nm. The fluorescence spectrum of **2** was observed, whereas neutral [6]MCPP exhibited negligible fluorescence due to forbidden transitions. The FWHM of the fluorescence band of **2** is also small (20 nm), comparable to that of quantum dots or dyes with heteroatoms.[16] No vibronic structure was observed in the fluorescence band, probably because the structure of **2** is too rigid to see obvious vibronic structures. The fluorescence quantum yield (Φ_F) of **2** is determined to be 0.23. Considering that the Stokes shift is only 5 nm and self-absorption is not negligible, the value of Φ_F is significant. Compared to [6]CPP^{2+} $(SbF_6^-)_2$ CH_2Cl_2 solution, **2** has over 10 times larger Φ_F (0.23 *vs.* 0.018).[4f] The oscillator strengths (f) for fluorescence of **2** and [6]CPP^{2+} $(SbF_6^-)_2$ were estimated to be 0.22 and 0.21, respectively, from TDDFT calculation based on the optimized structures of S_1 states for [6]MCPP^{2+} and [6]CPP^{2+} (see the Section 5 in ESI† for details). Because Φ_F is defined as $k_f/(k_f + k_{nr} + k_{ISC})$, where k_f is fluorescence rate, k_{nr} is nonradiative deactivation rate, k_{ISC} is intersystem crossing rate, and k_{ISC} is negligible for [6]MCPP^{2+} and [6]CPP^{2+}, the difference in Φ_F may be due to k_{nr}. Nonradiative deactivation, particularly thermal deactivation, is expected to be small in the [6]MCPP^{2+} scaffold compared to [6]CPP^{2+} by virtue of the rigid structure resulting from the methylene bridges. These results clearly show that methylene-bridging modulates the spectroscopic properties of the parent [6]CPP dication structure, enabling fluorescence, which is a remarkable structural effect of methylene-bridging firstly revealed by this work.

In our previous work, the paratropic belt current of MCPP, which changes depending on the ring size, was first unveiled.[12] The chemical shifts of the methylene hydrogen atoms in ^{1}H NMR spectra indicate the existence of a paratropic belt current that decreases with increasing ring size of [n]MCPP (n = 6, 8, and 10), which is also supported by a theoretical study of the magnetically induced current density. To investigate the belt-current effect in the [6]MCPP^{2+} scaffold, the ^{1}H NMR spectrum of **2** in CD_2Cl_2 was recorded (Fig. 4). As observed for neutral [6]MCPP, **2** also exhibited three types of signals: a singlet signal at 4.18 ppm, two doublet signals at 3.61 ppm and −0.34 ppm. This suggests a D_{3d} symmetry for **2** in CH_2Cl_2 solution, indicating a delocalized positive charge on the entire [6]MCPP^{2+} scaffold. The observed chemical shifts of the signals were further supported by simulations using gauge-including atomic orbitals (GIAO) calculations at the B3LYP/6-311+G(2d,p) level (see Section 5 in ESI† for details). The singlet signal of 4.18 ppm is assigned to the hydrogen atoms on benzene rings (highlighted as green color in Fig. 4). The doublet signal of 3.61 ppm is assigned to the methylene hydrogen atoms facing outside of nanobelt (H_{out}, highlighted as red color) and the doublet signal of −0.34 ppm is from those facing inside of nanobelt (H_{in}, highlighted as blue color).

A paratropic/diatropic belt current refers to a delocalized electronic current induced in cyclic π-conjugated molecules, such as nanobelts, when exposed to a magnetic field aligned with their symmetry axis. This current flows in a direction that

Open Access Article. Published on 23 April 2025. Downloaded on 6/3/2026 1:37:08 PM.
This article is licensed under a Creative Commons Attribution-NonCommercial 3.0 Unported Licence.

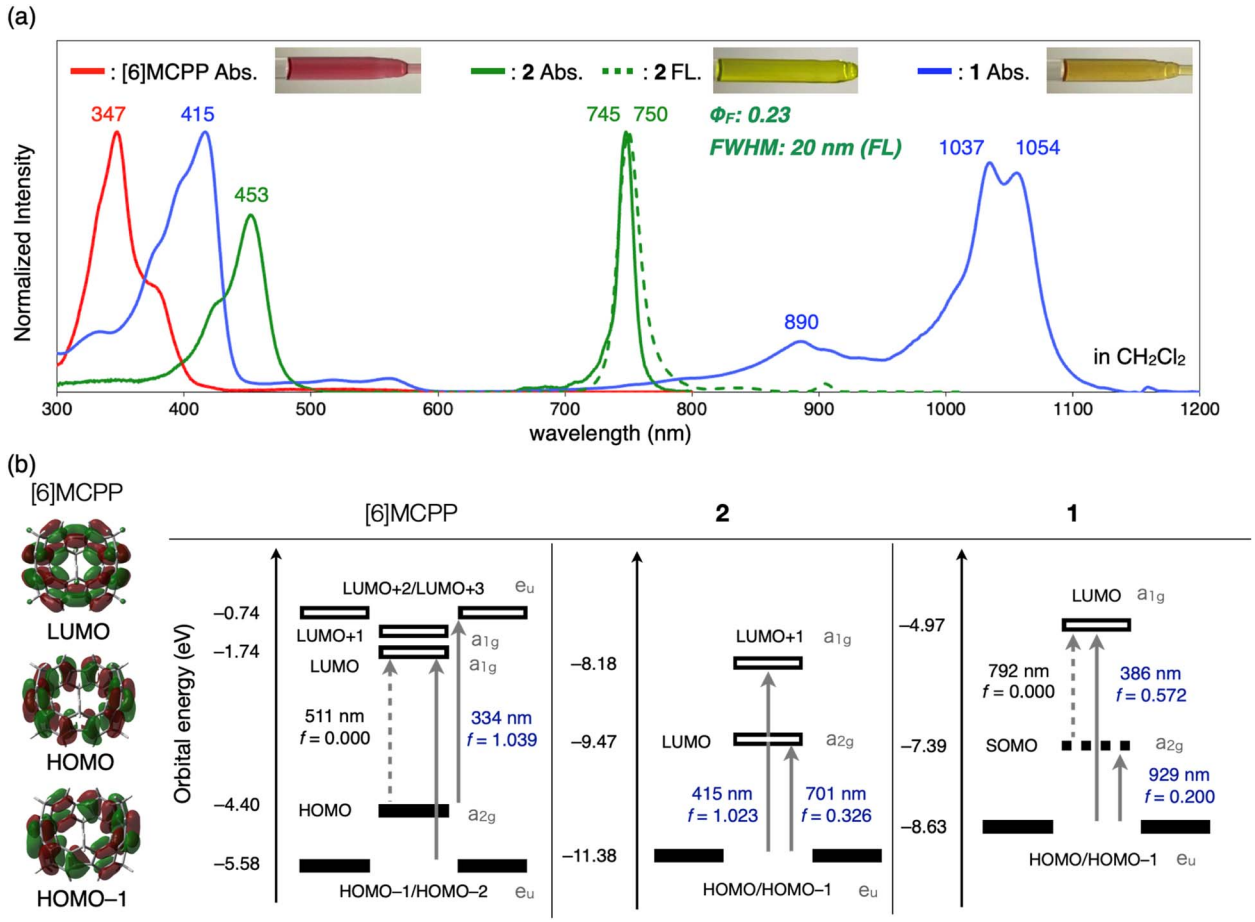

Fig. 3 (a) UV–vis–NIR absorption (solid line) and fluorescence (dashed line) spectra of CH_2Cl_2 solutions of [6]MCPP, **1**, and **2**. Fluorescence spectrum of **2** was recorded upon excitation at 450 nm. (b) Frontier molecular orbitals of [6]MCPP and transitions estimated by TDDFT calculation.

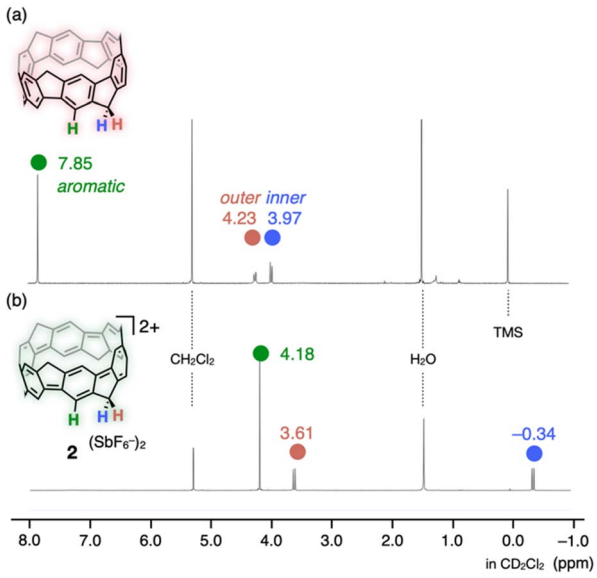

Fig. 4 ^{1}H NMR spectra of (a) [6]MCPP and (b) **2** at 600 MHz. TMS: tetramethylsilane.

generates a paramagnetic/diamagnetic (paratropic/diatropic) response, often associated with antiaromaticity/aromaticity.[12,17] As described in our previous reports concerning the neutral MCPP, ^{1}H NMR chemical shifts of hydrogen atoms, especially ones directed to inner side of the belt, provide evidence for the existence of the paratropic belt current in neutral MCPPs, further supported by a theoretical study of the magnetically induced current density. The extraordinary upfield shift of the ^{1}H NMR signals of **2** can only be attributed to a drastic change in the current regime induced by the magnetic field of the spectrometer. As we will show in the following, the paratropic belt current that characterizes the magnetic response of [6]MCPP disappears in the dication, giving way to an intense diatropic belt current that causes a large anisotropic effect on the ^{1}H NMR signals. The deshielding effect is particularly pronounced for H_{in}, whose δ moves up-field by 4.41 ppm. The aromatic hydrogen atoms undergo a similar shift equal to 3.67 ppm, while H_{out} moves only 0.62 ppm for their external disposition.

Magnetically-induced electron current density and aryl–aryl bond current strength of **2** have been calculated assuming the combination B97-2/6-311+G(2d,p) of density functional and

 © 2025 The Author(s). Published by the Royal Society of Chemistry

Open Access Article. Published on 23 April 2025. Downloaded on 6/3/2026 1:37:08 PM.
This article is licensed under a Creative Commons Attribution-NonCommercial 3.0 Unported Licence.

basis set, using the SYSMOIC program package as in previous studies, adopting the GSGT method for having origin-independent results.[17a] The wave functions for the calculation have been obtained using the G16 program package,[17b] including, in this case of a charged molecule, the solvent (CH_2Cl_2) effect by means of the CPCM method.[17c]

We find that the dominant contribution to the delocalized electron current density is given by the HOMO. This contribution is shown in Fig. 5, in which intensities lower than 0.04 a.u. were cut to clearly show the shape of the current and how its flow bifurcates and comes together around the six-membered rings of the nanobelts. To facilitate the comparison with [6]MCPP, we placed side by side in the bottom of Fig. 6 the current density calculated for the neutral (left) and charged (right) species adopting the same filter, this time equal to 0.015 a.u., to cut the low magnitude current. The inset on the left is therefore identical to that used for depiction of the paratropic belt current in [6]MCPP.

In comparison with [6]MCPP studied in ref. 12, first, we observe the opposite direction of circulation of the current, *i.e.*, diatropic instead of paratropic; second, the magnitude of the current is much larger. To obtain a quantitative estimate, bond current strengths[17d] have been calculated, integrating the current crossing a 5 × 5 a.u. square perpendicular to one aryl–aryl bond in its middle (shown in red in both Fig. 5 and 6) for the three instances: only HOMO, all-but-HOMO, all-MOs. Values are reported in Table 2 as a percentage of the benzene ring current strength (I_{BEN}) calculated using the same method, *i.e.*, $I/|I_{BEN}| \times 100$, with $I_{BEN} = 12$ nA T^{-1}. Customarily, the sign of the I_{BEN} is taken as negative, so that paratropic/diatropic current strengths are identified by a positive/negative sign.[17e]

As it can be seen, the delocalized diatropic belt current of **2** is almost entirely due to the HOMO. Two contributions were instead found for [6]MCPP, one dominant paratropic and another less intense diatropic. All that can be very easily understood by considering the symmetries of the frontier molecular orbitals shown in Fig. 3.

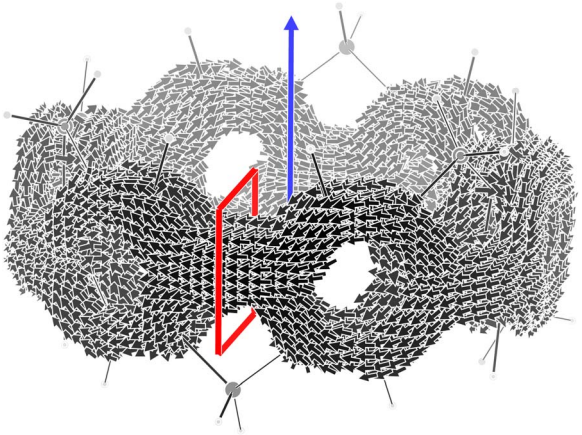

Fig. 5 HOMO contribution to the electron current density induced in **2** by a magnetic field parallel to the main symmetry axis (blue arrow). The current lower than 0.04 a.u. are not shown. Maximum current is 0.34 a.u. Red square delimits the integration region for the calculation of aryl–aryl bond current strength.

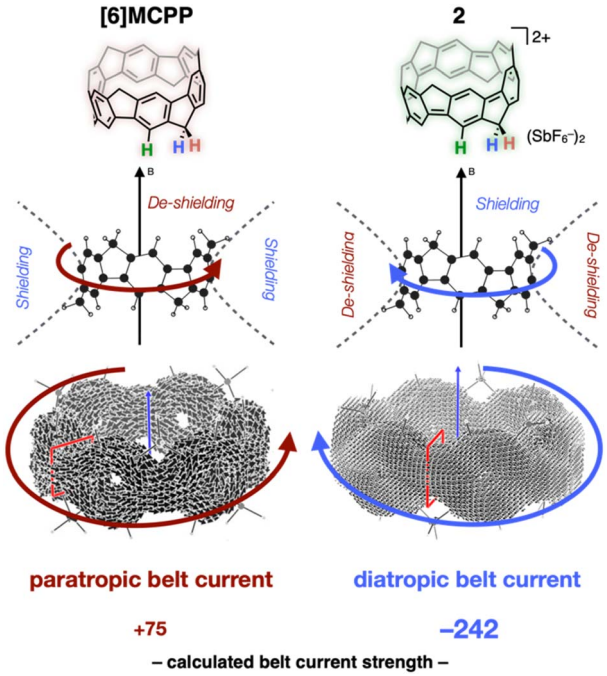

Fig. 6 The summary of belt current in neutral [6]MCPP (left) and [6]MCPP dication **2** (right). The belt current strength is calculated at B97-2/6-311+G(2d,p) level of theory adopting the CSGT method.

According to the few electrons model by Steiner and Fowler,[17f,g] an occupied-to-unoccupied virtual transition gives a paratropic contribution if the product of symmetries contains a match to a rotation, and a diatropic contribution if it contains a match to a translation. For [6]MCPP the HOMO → LUMO transition ($a_{2g} \times a_{1g} = a_{2g}$) gives the already well-known paratropic belt current whose strength is 138% of $|I_{BEN}|$, while the HOMO−1 → LUMO transition ($e_u \times a_{1g} = e_u$) makes a contribution that accounts almost entirely for the diatropic contribution of −63% of $|I_{BEN}|$. The smaller HOMO–LUMO gap is consistent with the bigger paratropic contribution. Now, as already observed above, the HOMO of [6]MCPP becomes the LUMO of **2**. Thus, two transitions originate from the HOMO of the dication ($e_u \times a_{2g} = e_u$ and $e_u \times a_{1g} = e_u$) which give the large diatropic belt current shown in Fig. 5, whose strength is estimated to be −242% of $|I_{BEN}|$.

The summary of the belt current of neutral [6]MCPP and **2** is shown in Fig. 6. Two-electron oxidation turns a paratropic belt current of MCPP skeleton into a diatropic belt current, which is significantly increased to reflect experimentally observed huge

Table 2 Belt signed current strength (aryl–aryl) in percentage of the benzene ring current strength calculated using the same method

Molecule	HOMO	All-but-HOMO	All-MOs
2	−241	−1	−242
[6]MCPP	+138	−63	+75

Open Access Article. Published on 23 April 2025. Downloaded on 6/3/2026 1:37:08 PM.
This article is licensed under a Creative Commons Attribution-NonCommercial 3.0 Unported Licence.

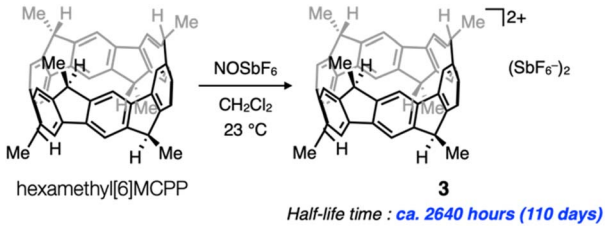

Scheme 2 Chemical oxidation of hexamethyl[6]MCPP. Reaction conditions: hexamethyl[6]MCPP (7.6 μmol, 4.6 mg, 1.0 equiv.), $NOSbF_6$ (23 μmol, 6.0 mg, 3.0 equiv.), CH_2Cl_2 (3.0 mL). Half-life time was elucidated in CH_2Cl_2 solution at 23 °C under air.

upfield ^{1}H NMR chemical shift of inner methylene hydrogen atoms of **2**. Owing to the large strength of the diatropic belt current in the dication, the current predicted based on the "in-plane aromaticity" concept[4c] appears to be qualitatively correct. The belt current has a sizable effect also on the carbon NMR signals (see Tables S5–S9 in ESI† for a brief account). In addition, nucleus-independent chemical shift (NICS) was also calculated, which also indicates the increased aromaticity of **2** (see Table S4 in ESI†).

The interesting properties of **1** and **2** described above are unveiled owing to their high stability under air as both solution and solid. In order to discuss the extraordinarily high stability of **2**, the chemical oxidation of hexamethyl[6]MCPP, which is a known molecule reported in 2021,[14a] has been tried in a same manner as the synthesis of **2** (Scheme 2). The dicationic species of hexamethyl[6]MCPP **3** has been obtained successfully to investigate its half-life time in CH_2Cl_2 solution under air. As a result, it was found that **3** has a much longer half-life time than **2**, which is estimated to be about 2640 hours (110 days). Although discussion for high stability was difficult because neither ^{13}C NMR analysis nor X-ray diffraction analysis was successful, kinetic protection, electron-donating effect and hyperconjugation effect of methyl groups likely improve the stability of [6]MCPP dication.

Conclusions

In conclusion, we have synthesized [6]MCPP radical cationic salt **1** and [6]MCPP dicationic salt **2** from [6]MCPP. The appropriate choice of chemical oxidants has led the successful synthesis of the [6]MCPP cationic species. The half-life times of the cationic species are longer than those of CPP cationic species, possibly owing to the methylene-bridged structures which fix the quinoidal CPP structure to a belt form. As important properties of [6]MCPP cations, we found that the crystal structure of **2** has an obvious quinoidal character and a smaller diameter in contrast to neutral [6]MCPP. The UV–vis–NIR absorption and fluorescence spectra of **2** have small FWHM in long wavelength close to NIR, which indicates the possibility of **2** to be used as a unique photo material. The drastic change in the fluorescence quantum yields of **2** ($\Phi_F = 0.23$) and neutral [6]MCPP ($\Phi_F \sim 0$) means that turning the fluorescence on and off is possible by using oxidation of [6]MCPP. Notably, experimental and theoretical ^{1}H NMR studies of **2** uncovered its interesting magnetic property: a diatropic belt current. The belt current of **2** is much stronger than that of [6]MCPP, which is reasonable from allowed transition in frontier molecular orbitals of **2**. The diatropic belt current should be present in already reported [*n*]CPP dications; however, evidence for it is difficult to obtain without the characteristic methylene hydrogen atoms in **2**, the ^{1}H NMR chemical shifts of which are strongly affected by the diatropic belt current. In order to create highly stable MCPP dications, hexamethyl[6]MCPP has been oxidized similarly. The thus-obtained dication **3** was extraordinarily stable to strongly indicate the hyperconjugation effect, electron-donating effect and kinetic protection by the methyl groups in **3**. The compounds synthesized in this study are remarkably stable radical and cationic nanobelts. Their striking properties would give new insights into the chemistry of π-conjugated molecules and materials science.

Data availability

The data that support the findings of this study are available in the ESI† of this article.

Author contributions

A. Y. and K. I. conceived the concept and directed the project. N. K. and H. K. synthesized compounds **1**, **2**, **3** and performed all experimental measurements and DFT calculations. T. S. contributed to synthesize compound **3**. D. I. performed and analyzed X-ray crystallography. R. Z., G. M. and F. F. S. performed the DFT calculations for NMR studies. R. Z., L. T. S., A. Y., and K. I. wrote the manuscript with feedback from other authors. All authors approved the final version of the manuscript.

Conflicts of interest

There are no conflicts to declare.

Acknowledgements

We thank Dr Kin-ichi Oyama and Ms. Rio Yamada (Nagoya University) for their support in ESI-MS measurement and analysis. We also thank Ms Yui Ito, Associate Prof. Masahito Murai and Prof. Shigehiro Yamaguchi (Nagoya University) for their support in NIR absorption and FL measurements. The authors also thank Dr Hiroki Shudo (Nagoya University) for fruitful discussion. We also thank the referees of our first manuscript for their valuable suggestions. H. K. and D. I. thank the Nagoya University Graduate Program of Transformative Chem-Bio Research (WISE Program) supported by MEXT. T. S. thanks and the Deutsche Forschungsgemeischaft (DFG, German Research Foundation – GRK2678-437785492). Computations were performed using the resources of the Research Center for Computational Science, Okazaki, Japan (23-IMS-C087 and 24-IMS-C123). This work is supported by JSPS Promotion of Joint International Research (grant number

 © 2025 The Author(s). Published by the Royal Society of Chemistry

Open Access Article. Published on 23 April 2025. Downloaded on 6/3/2026 1:37:08 PM. This article is licensed under a Creative Commons Attribution-NonCommercial 3.0 Unported Licence.

22K21346 to A. Y.), JSPS KAKENHI (grant number 19H05463 to K. I.) and Sumitomo Foundation (to A. Y.).

Notes and references

1 (*a*) K. S. Peters, *Chem. Rev.*, 2007, **107**, 859–873; (*b*) J. Heinze, B. A. Frontana-Uribe and S. Ludwigs, *Chem. Rev.*, 2010, **110**, 4724–4771; (*c*) J. Bosson, J. Gouin and J. Lacour, *Chem. Soc. Rev.*, 2014, **43**, 2824–2840; (*d*) K. Goossens, K. Lava, C. W. Bielawski and K. Binnemans, *Chem. Rev.*, 2016, **116**, 4643–4807; (*e*) N. A. Romero and D. A. Nicewicz, *Chem. Rev.*, 2016, **116**, 10075–10166.

2 (*a*) T. Nishinaga *Organic Redox Systems*, John Wiley & Sons, Inc, Hoboken, NJ, 2015; (*b*) P. W. Antoni and M. M. Hansmann, *J. Am. Chem. Soc.*, 2018, **140**, 14823–14835; (*c*) T. Harimoto and Y. Ishigaki, *ChemPlusChem*, 2022, **87**, e202200013.

3 (*a*) A. Matsuura, T. Nishinaga and K. Komatsu, *J. Am. Chem. Soc.*, 2000, **122**, 10007–10016; (*b*) K. Komatsu, S. Aonuma, Y. Jinbu, R. Tsuji, C. Hirosawa and K. Takeuchi, *J. Org. Chem.*, 1991, **56**, 195–203; (*c*) M. Banerjee, V. S. Vyas, S. V. Lindeman and R. Rathore, *Chem. Commun.*, 2008, 1889–1891; (*d*) M. Banerjee, R. Shukla and R. Rathore, *J. Am. Chem. Soc.*, 2009, **131**, 1780–1786; (*e*) T. Nishiuchi, S. Aibara and T. Kubo, *Angew. Chem., Int. Ed.*, 2018, **57**, 16516–16519; (*f*) C. Zhu, K. Shoyama and F. Würthner, *Angew. Chem., Int. Ed.*, 2020, **59**, 21505–21509; (*g*) Y. Ishigaki, T. Harimoto, K. Sugawara and T. Suzuki, *J. Am. Chem. Soc.*, 2021, **143**, 3306–3311; (*h*) H. Miyoshi, R. Sugiura, R. Kishi, S. N. Spisak, Z. Wei, A. Muranaka, M. Uchiyama, N. Kobayashi, S. Chatterjee, Y. Ie, I. Hisaki, M. A. Petrukhina, T. Nishinaga, M. Nakano and Y. Tobe, *Angew. Chem., Int. Ed.*, 2022, **61**, e202115316; (*i*) Z. Li, X. Hou, Y. Han, W. Fan, Y. Ni, Q. Zhou, J. Zhu, S. Wu, K. Huang and J. Wu, *Angew. Chem., Int. Ed.*, 2022, **61**, e202210697; (*j*) T. Yoshihara, H. Shudo, A. Yagi and K. Itami, *J. Am. Chem. Soc.*, 2023, **145**, 11754–11763.

4 (*a*) M. R. Golder, B. M. Wong and R. Jasti, *Chem. Sci.*, 2013, **4**, 4285–4291; (*b*) E. Kayahara, T. Kouyama, T. Kato, H. Takaya, N. Yasuda and S. Yamago, *Angew. Chem., Int. Ed.*, 2013, **52**, 13722–13726; (*c*) N. Toriumi, A. Muranaka, E. Kayahara, S. Yamago and M. Uchiyama, *J. Am. Chem. Soc.*, 2015, **137**, 82–85; (*d*) E. Kayahara, T. Kouyama, T. Kato and S. Yamago, *J. Am. Chem. Soc.*, 2016, **138**, 338–344; (*e*) M. P. Alvarez, M. C. Ruiz Delgado, M. Taravillo, V. G. Baonza, J. T. López Navarrete, P. Evans, R. Jasti, S. Yamago, M. Kertesz and J. Casado, *Chem. Sci.*, 2016, **7**, 3494–3499; (*f*) Y. Masumoto, N. Toriumi, A. Muranaka, E. Kayahara, S. Yamago and M. Uchiyama, *J. Phys. Chem. A*, 2018, **122**, 5162–5167; (*g*) E. R. Darzi, E. S. Hirst, C. D. Weber, L. N. Zakharov, M. C. Lonergan and R. Jasti, *ACS Cent. Sci.*, 2015, **1**, 335–342; (*h*) J. M. Van Raden, E. R. Darzi, L. N. Zakharov and R. Jasti, *Org. Biomol. Chem.*, 2016, **14**, 5721–5727; (*i*) F. Schwer, S. Zank, M. Freiberger, R. Kaur, S. Frühwald, C. C. Robertson, A. Görling, T. Drewello, D. M. Guldi and M. von Delius, *Org. Mater.*, 2022, **4**, 7–17.

5 (*a*) Y. Segawa, H. Ito and K. Itami, *Nat. Rev. Mater.*, 2016, **1**, 15002; (*b*) Y. Segawa, D. R. Levine and K. Itami, *Acc. Chem. Res.*, 2019, **52**, 2760–2767; (*c*) N. Panwar, A. M. Soehartono, K. K. Chan, S. Zeng, G. Xu, J. Qu, P. Coquet, K. Yong and X. Chen, *Chem. Rev.*, 2019, **119**, 9559–9656; (*d*) A. Tielens, *Annu. Rev. Astron. Astrophys.*, 2008, **46**, 289–337; (*e*) R. G. Harvey *Polycyclic Aromatic Hydrocarbons*, Wiley-VCH, New York, 1997; (*f*) A. Narita, X. Wang, X. Feng and K. Müllen, *Chem. Soc. Rev.*, 2015, **44**, 6616–6643; (*g*) K. Yoon and G. Dong, *Mater. Chem. Front.*, 2020, **4**, 29–45.

6 G. Povie, Y. Segawa, T. Nishihara, Y. Miyauchi and K. Itami, *Science*, 2017, **356**, 172–175.

7 (*a*) S. E. Lewis, *Chem. Soc. Rev.*, 2015, **44**, 2221–2304; (*b*) Y. Segawa, A. Yagi, K. Matsui and K. Itami, *Angew. Chem., Int. Ed.*, 2016, **55**, 5136–5158; (*c*) Q. Guo, Y. Qiu, M. Wang and J. Fraser Stoddart, *Nat. Chem.*, 2021, **13**, 402–419; (*d*) D. Imoto, A. Yagi and K. Itami, *Precis. Chem.*, 2023, **1**, 516–523.

8 (*a*) X. Lu, T. Y. Gopalakrishna, Y. Han, Y. Ni, Y. Zou and J. Wu, *J. Am. Chem. Soc.*, 2019, **141**, 5934–5941; (*b*) H. Sato, R. Suizu, T. Kato, A. Yagi, Y. Segawa, K. Awaga and K. Itami, *Chem. Sci.*, 2022, **13**, 9947–9951.

9 Y. Li, Y. Segawa, A. Yagi and K. Itami, *J. Am. Chem. Soc.*, 2020, **142**, 12850–12856.

10 (*a*) T. Ogoshi, S. Kanai, S. Fujinami, T. Yamagishi and Y. Nakamoto, *J. Am. Chem. Soc.*, 2008, **130**, 5022–5023; (*b*) T. Ogoshi, T. Yamagishi and Y. Nakamoto, *Chem. Rev.*, 2016, **116**, 7937–8002.

11 https://www.tcichemicals.com/assets/brochure-pdfs/Brochure_FF122_E.pdf.

12 H. Kono, Y. Li, R. Zanasi, G. Monaco, F. F. Summa, L. T. Scott, A. Yagi and K. Itami, *J. Am. Chem. Soc.*, 2023, **145**, 8939–8946.

13 N. Kai, H. Kono, A. Yagi and K. Itami, *Synlett*, 2023, **34**, 1433–1436.

14 (*a*) X. Du, D. Zhang, Y. Guo, J. Li, Y. Han and C. Chen, *Angew. Chem., Int. Ed.*, 2021, **60**, 13021–13028; (*b*) F. Zhang, X. Du, D. Zhang, Y. Wang, H. Lu and C. Chen, *Angew. Chem., Int. Ed.*, 2021, **60**, 15291–15295.

15 CCDC number of **2**: 2359239.

16 (*a*) J. M. Pietryga, Y. Park, J. Lim, A. F. Fidler, W. K. Bae, S. Brovelli and V. I. Klimov, *Chem. Rev.*, 2016, **116**, 10513–10622; (*b*) W. Zhao and E. M. Carreira, *Angew. Chem., Int. Ed.*, 2005, **44**, 1677–1679.

17 (*a*) G. Monaco, F. F. Summa and R. Zanasi, *J. Chem. Inf. Model.*, 2021, **61**, 270–283; (*b*) M. J. Frisch, G. W. Trucks, H. B. Schlegel, G. E. Scuseria, M. A. Robb, J. R. Cheeseman, G. Scalmani, V. Barone, G. A. Petersson, H. Nakatsuji, X. Li, M. Caricato, A. V. Marenich, J. Bloino, B. G. Janesko, R. Gomperts, B. Mennucci, H. P. Hratchian, J. V. Ortiz, A. F. Izmaylov, J. L. Sonnenberg, D. Williams-Young, F. Ding, F. Lipparini, F. Egidi, J. Goings, B. Peng, A. Petrone, T. Henderson, D. Ranasinghe, V. G. Zakrzewski, J. Gao, N. Rega, G. Zheng, W. Liang, M. Hada, M. Ehara, K. Toyota, R. Fukuda, J. Hasegawa, M. Ishida, T. Nakajima, Y. Honda, O. Kitao, H. Nakai, T. Vreven, K. Throssell, J. A. Montgomery Jr, J. E. Peralta,

Open Access Article. Published on 23 April 2025. Downloaded on 6/3/2026 1:37:08 PM.
This article is licensed under a Creative Commons Attribution-NonCommercial 3.0 Unported Licence.

F. Ogliaro, M. J. Bearpark, J. J. Heyd, E. N. Brothers, K. N. Kudin, V. N. Staroverov, T. A. Keith, R. Kobayashi, J. Normand, K. Raghavachari, A. P. Rendell, J. C. Burant, S. S. Iyengar, J. Tomasi, M. Cossi, J. M. Millam, M. Klene, C. Adamo, R. Cammi, J. W. Ochterski, R. L. Martin, K. Morokuma, O. Farkas, J. B. Foresman and D. J. Fox, *Gaussian 16, Revision C.01*, Gaussian, Inc., Wallingford CT, 2019; (*c*) M. Cossi, N. Rega, G. Scalmani and V. Barone, *J. Comput. Chem.*, 2003, **24**, 669–681; (*d*) J. Jusélius, D. Sundholm and J. Gauss, *J. Chem. Phys.*, 2004, **121**, 3952–3963; (*e*) G. Monaco and R. Zanasi, *J. Phys. Chem. A*, 2014, **118**, 1673–1683; (*f*) E. Steiner and P. W. Fowler, *J. Phys. Chem. A*, 2001, **105**, 9553–9562; (*g*) E. Steiner and P. W. Fowler, *Chem. Commun.*, 2001, **21**, 2220–2221.

 © 2025 The Author(s). Published by the Royal Society of Chemistry